Using $\mathfrak{M}=e(2k)^{-1/2}M$, the decay rate R is then given by

$$R=\tfrac{16}{27}\alpha(k^3/m^4)I^2. \quad (11)$$

We have evaluated I using six-parameter variational helium wave functions computed by Huang.[6] The result obtained is $I=-(\frac{1}{4}\alpha^2 m)(1.87)$. Using $kc=2.99\times10^{16}$ Hz, we then get $R=1.2\times10^{-4}$ sec^{-1} or a helium lifetime

$$\tau=8.4\times10^{3} \text{ sec}. \quad (12)$$

We have also evaluated the decay rate in the limit of heliumlike ions with very high Z, where the wave functions are taken as products of hydrogenic wave functions, and find

$$R=\tfrac{4}{2187}Z^8\alpha^9 k. \quad (13)$$

We thank Dr. Dennis Sciama and Dr. Hans Griem for stimulating our interest in this problem, and Mr. Ralph Grishman for aid in the numerical calculations. One of us (J.S.) would like to thank Dr. E. Henley and the Physics Department of the University of Washington for their hospitality during the summer of 1970 when part of this work was done.

*Work supported in part by the U. S. Air Force Office of Scientific Research under Grant No. AFOSR 68-1453MOD# C and the U. S. Atomic Energy Commission.

[1]See M. J. Rees and D. W. Sciama, Comm. Astrophys. Space Phys. 1, 35 (1969).

[2]A. H. Gabriel and C. Jordan, Nature 221, 947 (1969); H. R. Griem, Astrophys. J. 156, L103 (1969), and 161, L155 (1970).

[3]R. W. Schmieder and R. Marrus, Phys. Rev. Lett. 25, 1245 (1970).

[4]See, e.g., H. Bethe and E. Salpeter, *Quantum Mechanics of One- and Two-Electron Atoms* (Springer, Berlin, 1957), p. 173. In addition, it is questionable whether H_{DB} has any normalizable eigenstates at all because of the nondenumerable degeneracy of the spectrum in the absence of electron-electron interaction.

[5]After this work was completed, we were informed of the work of G. Drake (to be published) who also has obtained (9) and has carried out numerical evaluations of (9) with many-parameter wave functions for a variety of values of Z. However, this author's starting point is a Hamiltonian containing both the Breit operator B and H_T which has no theoretical foundation; in fact, it gives the wrong fine structure, since H_T is the source of B and transverse photon effects are being counted twice. Drake's numerical result for helium is in substantial agreement with ours.

[6]S. Huang, Astrophys. J. 108, 354 (1948).

X-Ray Parametric Conversion

P. Eisenberger and S. L. McCall
Bell Telephone Laboratories, Murray Hill, New Jersey 07974
(Received 30 December 1970)

The observation of x-ray parametric conversion is reported. Results are in accord with the calculated nonlinear x-ray susceptibility. The appropriate nonlinear mechanisms are described in terms of classical free electrons.

An x-ray nonlinear optical effect has been observed and the corresponding second-order susceptibility measured. Parametric conversion is the absorption of a photon at frequency ω_p with the resultant emission of two photons of frequencies ω_1 and ω_2, where $\omega_1+\omega_2=\omega_p$. At visible wave lengths,[1,2] this phenomena has been observed and measured in a number of materials. Motivated by Freund and Levine's proposal and calculations,[3] we have observed the analogous phenomena in the x-ray regime.

As shown in Fig. 1, the filtered and collimated output of a 2-kW x-ray tube emitting characteristic molybdenum radiation at 17 keV intercepted a beryllium crystal almost oriented for $(11\bar{2}0)$ Bragg scattering. The outgoing radiation was analyzed for coincident photon pairs with energy near 8.5 keV. The observed coincident counting rates were peaked in directions determined by energy-momentum conservation. The measured cross section is in accord with calculations.[3]

Electrons may be regarded as free if $\hbar\omega_p$, $\hbar\omega_1$, $\hbar\omega_2 \gg E_B$, where E_B is a typical electron binding energy. Relativistic effects are small if $\hbar\omega_p \ll mc^2$. In the experiment described here, $\hbar\omega_p = 17$ keV, and $E_B \sim 100$ eV.

Optical nonlinear[4] phenomena depend qualitatively on such material properties as inversion asymmetry and resonances. In contrast, nonlinear x-ray mechanisms involving only x-ray photons depend primarily on the properties of free electrons. Gross material properties, such as

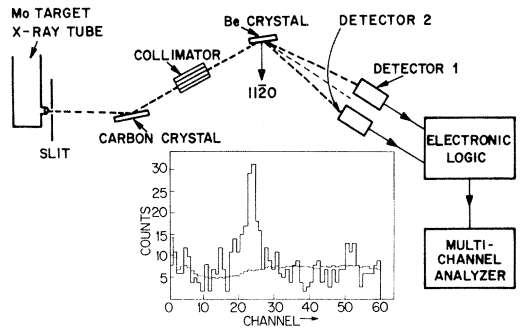

FIG. 1. Experimental apparatus. The sample-detector distance was 16 in., of which 12 in. was a helium path provided by a tube with 0.000 25-in. Mylar windows. Shielding insured that only the photon path shown was possible. The insert (200 nsec total) shows energy-selected time-correlation spectra. The smooth spectrum is due to random events, and the peaked spectrum represents the total data for the three points near $\delta\theta_B = +15'$ in Fig. 2(a).

electron densities or absorption constants, are important only in determining the magnitude of the nonlinearity.

The parametric process may be understood in terms of the inverse process, wherein two photons at frequencies ω_1 and ω_2 beat to form a photon at frequency ω_p, since the same matrix element is involved in both processes. We will adopt this viewpoint and consider sum-frequency generation. A classical calculation of the response of free electrons[5,6] to two incident fields $(\vec{E}_1, \vec{B}_1)$ and $(\vec{E}_2, \vec{B}_2)$ leads to the identification of three specific nonlinear effects. An electron is driven by the applied electric fields $\vec{E}_1$ and $\vec{E}_2$. Due to field $\vec{E}_1$, the electron acquires a velocity $\vec{v}_1$ and displacement $\vec{x}_1$. The Lorentz-force component $\vec{v}_1 \times \vec{B}_2$ leads to a second-order velocity with frequency components at $\omega_p = \omega_1 + \omega_2$. The displacement $\vec{x}_1$ results in the electron sampling a different portion of the field $\vec{E}_2$, which also leads to a second-order velocity. Finally, the electron moving with velocity component $\vec{v}_1$ reflects the field $\vec{E}_2$. The Doppler-shifted reflected field has sum-frequency components.

Let an electron be driven by fields $\vec{E}_1$ and $\vec{E}_2$, and define $\vec{E}_1 = \vec{E}_1^{+} + \vec{E}_1^{-}$, with $\vec{E}_1^{\pm}$ varying as $\exp[\pm i(\vec{k}_1 \cdot \vec{r} - \omega_1 t)]$. The Lorentz equation

$$\dot{\vec{v}} = -(e/m)(\vec{E} + \vec{v} \times \vec{B}/c), \tag{1}$$

where $\vec{v}$ is the electron velocity, $\vec{E} = \vec{E}_1 + \vec{E}_2$, and $\vec{B}$ is the associated magnetic field, may be solved to first order in $eE/m\omega_1 c$ to yield

$$\vec{v}^{(1)} = -ie\vec{E}_1^{+}/m\omega_1 + \cdots; \tag{2}$$

here and in the following, "$\cdots$" means that terms with subscripts 1 and 2 interchanged and complex conjugate terms are to be added. The corresponding displacement is

$$\vec{r}^{(1)} = e\vec{E}_1^{+}/m\omega_1^2 + \cdots. \tag{3}$$

These quantities may be substituted into the Lorentz equation to find the second-order velocity at the sum frequency ω_p:

$$\vec{v}^{(2)} = -\left(\frac{e}{m}\right)^2 \left[\frac{\vec{E}_1^{+} \times (\vec{k}_2 \times \vec{E}_2^{+})}{\omega_1 \omega_2 \omega_p} - \frac{(\vec{E}_1^{+} \cdot \vec{k}_2)\vec{E}_2^{+}}{\omega_1^2 \omega_p} + \cdots\right]. \tag{4}$$

The second-order current density is

$$\vec{J}^{(2)} = -e\vec{v}^{(2)}\delta(\vec{r} - \vec{r}_0) - e\vec{v}^{(1)}[\delta(\vec{r} - \vec{r}_0 - \vec{r}^{(1)}) - \delta(\vec{r} - \vec{r}_0)], \tag{5}$$

where, in the second term, only the terms to first order in $\vec{r}^{(1)}$ are kept. Here $\vec{r}_0$ is the initial position of the electron.

The average value of $\vec{J}^{(2)}$ is found by averaging over position $\vec{r}_0$ and summing over electrons. The resultant average nonlinear current density is

$$\langle \vec{J}^{(2)} \rangle = \frac{e^3}{m^2}\left[\frac{\vec{E}_1^{+} \times (\vec{k}_2 \times \vec{E}_2^{+})}{\omega_1 \omega_2 \omega_p} - \frac{(\vec{E}_1^{+} \cdot \vec{k}_2)\vec{E}_2^{+}}{\omega_1^2 \omega_p}\right]\rho(\vec{r}) - i\frac{e^3}{m^2}\frac{(\vec{E}_1^{+} \cdot \nabla)\rho(\vec{r})\vec{E}_2^{+}}{\omega_1^2 \omega_2} + \cdots, \tag{6}$$

where $\rho(\vec{r})$ is the electron density at point $\vec{r}$. The three terms represent respectively, the nonlinear Lorentz, displacement, and Doppler terms. In the experiment discussed here, the displacement term was relatively unimportant because $\vec{k}_1$ and $\vec{k}_2$ were approximately parallel.

When a reciprocal lattice vector $\vec{G}$ determines a discrete Fourier component $\rho(\vec{G})$ of the charge density, the resultant radiation can only be nonzero if $\vec{k}_1 + \vec{k}_2 = \vec{k}_p + \vec{G}$, and $\omega_p = \omega_p + \omega_2$. These are the phase-matching or energy-momentum-

conservation conditions. Under such circumstances, the above expression for current reduces to Freund and Levine's result[3] through the defining relation for polarization, $\vec{P}=\vec{J}$.

It is illustrative to regard spontaneous parametric fluorescence as the result of input x rays at frequency ω_p beating with zero-point fluctuations at frequencies ω_1 and ω_2 to produce real photons at frequencies ω_2 and ω_1. The zero-point fluctuation of the photon field with a frequency less than ω may be identified with a flux $\hbar\omega^4/32\pi^2c^2$ erg/cm^2 sec, which at x-ray frequencies is very large (e.g., 5×10^{19} W/cm^2 for ω corresponding to 1-Å radiation) and compensates for the smallness of the nonlinear coefficients.

The Bragg-scattering condition is $|\vec{k}_p+\vec{G}|=|\vec{k}_p|$. If the crystal is turned through a small angle $\delta\theta_B$ away from the Bragg-scattering condition, so that $|\vec{k}_p+\vec{G}|<|\vec{k}_p|$, a parametric photon pair may be created. Two photons with energies $x\hbar\omega_p$ and $y\hbar\omega_p$, $x+y=1$, are emitted at angles $R(x)$ and $R(y)$ with respect to the Bragg direction k_p+G, where, as a consequence of energy-momentum conservation,

$$R(x)=[2\delta\theta_B(y/x)\sin2\theta_B]^{1/2}. \quad (7)$$

Here θ_B is the Bragg angle determined by $\vec{k}_p\cdot(\vec{k}_p+\vec{G})=|\vec{k}_p||\vec{k}_p+\vec{G}|\cos2\theta_B$. A view towards the crystal along the direction of Bragg scattering presents a series of circles of angular radii $R(x)$ centered on the Bragg direction $\vec{k}_p+\vec{G}$. A parametric photon pair with angular radii $R(x)$ and $R(y)$ will come out at angles φ and $\varphi+\pi$ with respect to the direction defined by the intersection of the plane perpendicular to the Bragg-scattering direction and the plane defined by $\vec{k}_p$ and $\vec{G}$. Parametrically scattered pairs will only be detected when one detector is positioned to intercept $R(x)$ and an opposite position with respect to the Bragg direction intercepts $R(y)$.

The cross-section formula[3] has the form

$$d\sigma/d\Omega\propto[R(x)+R(y)]^{-2}, \quad (8)$$

and thus the cross section varies approximately as $[R(\frac{1}{2})]^{-2}$, since $x,y\approx\frac{1}{2}$. The solid angle $d\Omega$ into which the parametric photons are scattered is roughly given by $\pi[R(\frac{1}{2})]^2$. Thus the total cross section is independent of $\delta\theta_B{}^{-1}$, even though Eq. (8) specifies an intensity which increases as $\delta\theta_B{}^{-1}$.

Input photons which Compton scatter from the Be crystal produce a large flux in each detector which is proportional to Ω_d, the solid angle of the detectors. By use of a small $\delta\theta_B$, a small detector solid angle can be used without signal reduction, but with a reduction in the Compton background. Beryllium was chosen because its crystal perfection was adequate to work at small $\delta\theta_B$ and because its low x-ray absorption constant allows a large interaction volume. With $\delta\theta_B=15'$ and $\Omega_d=0.0021$ sr the Compton background was still 2500 sec^{-1}. The signal rate finally detected was about 1 h^{-1}. The Compton background, which is random in time with energies near 17 keV, was discriminated against by detecting only coincident events involving photons with measured energies between 5 and 11 keV.

We used Integral Line 1-in.-diam NaI-Th scintillator detectors with 250-nsec fluorescent lifetimes and an efficiency of three photoelectrons from the photomultiplier cathode for each keV of absorbed energy. These detectors had a timing-pulse limitation of one photoelectron per 10 nsec at the leading edge of a pulse associated with the absorption of an 8.5-keV photon.

The photomultiplier outputs were capacitatively probed for timing pulses, which were processed by a time-to-pulse-height converter. The photomuliplier outputs were also integrated and the energy inspected. Approximately 98% of the 17-keV Compton-scattered photons were rejected by the energy analysis. If the energy pulses were appropriate for x rays in the energy range of 5-11 keV, and if a pile-up rejecting circuit did not veto, then the time-to-pulse-height converter output was stored in a multichannel-analyzer memory. The efficiency of the detectors and electronics was measured by observing coincidences provided by a 10-nsec pulsed copper anode x-ray tube constructed for that purpose. Dead time was adjusted for a 10% signal loss.

In Fig. 1 a coincidence profile due to randomly occuring x rays is illustrated together with the profile obtained under detection of real coincidences. The random profile was used to calibrate the channel-number scale into time delays by measurement of the singles rate in each detector. The coincident channel, zero time delay, was determined from measurements on a Na^{22} source. The total signal was obtained by adding without weight the counts corresponding to a time of 52 nsec centered around the coincident time. Background was subtracted according to the calculated random coincident rate due to the measured-singles counting rate, $N_B=N_1N_2\tau$, where N_1 and N_2 are the singles rates of the two detectors and τ is the 52-nsec time interval which, according to energy-selected Na^{22} coincidences,

contained 90% of the signal. The combined effects of energy discrimination and coincident counting resulted in a decrease of the 17-keV random Compton-background signal of 2.5×10^{3} $\sec^{-1}$ at each detector to less than 3×10^{-4} $\sec^{-1}$ in the 52-nsec coincident region.

The beam leaving the collimator (see Fig. 1) was composed mainly of $K\alpha_1$ and $K\alpha_2$ characteristic molybdenum radiation and had a divergence of approximately 6′ in the Bragg plane and 30′ perpendicular to it. The beam directly illuminated the 1-in.-diam cut face of a beryllium crystal boule, with a $11\bar{2}0$ ($\bar{a}$ axis) crystal lattice vector ($2\theta_B = 36.25°$) about 30° away from the face normal. The orientation of the boule was such that the input beam made an angle of 9° with the face. "Glancing geometry"[3] provided only an increase of 1.5 in the signal-to-noise ratio because of the increased background and beam-size magnification which results from its use. The $\bar{a}$ axis pointed about 20° away from the plane defined by the input and face normal directions. The collimator slits were tilted to minimize the Bragg-scattering-plane divergence.

According to the energy-momentum conservation argument, coincidences should only be observed when the crystal is oriented so that $|\vec{k}_p + \vec{G}| < |\vec{k}_p|$, since $|\vec{k}_1 + \vec{k}_2| < |\vec{k}_1| + |\vec{k}_2| = |\vec{k}_p|$. Furthermore, the peak counting rate should occur when $\delta\theta_B$ is such that $R(\frac{1}{2})$ is approximately equal to the corresponding angle determined by the detector position. The data in Fig. 2(a) were obtained by varying $\delta\theta_B$ while the detector positions were held fixed in the Bragg scattering plane determined by $\vec{k}_p$ and $\vec{G}$, at positions corresponding to $R(\frac{1}{2})$ for $\delta\theta_B = 15'$. The data are the results of about 50 runs with each run about 8 h in duration, and the sequence of values of $\delta\theta_B$ was determined by a random process.

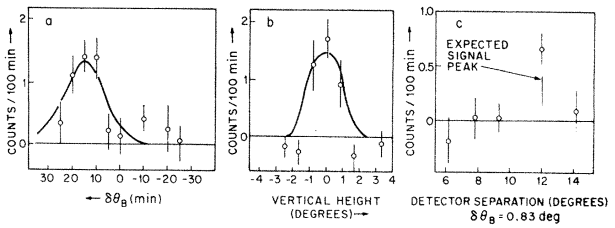

FIG. 2. Experimental and theoretical (solid line) results. In (a) the detector separation was adjusted for a $\delta\theta_B$ of 15′. The coincidence signal was measured for various $\delta\theta_B$. In (b) the crystal was set at $\delta\theta_B = 15'$; the detector separation was held at same value as in (a), but the detectors were moved together in a direction perpendicular to the Bragg plane. In (c) the crystal was set at $\delta\theta_B = 0.83°$ and the detector separation in the Bragg plane was changed keeping the Bragg spot equidistant between the detectors. The observed signal ocurred only when Eq. (7) was satisfied.

The results of similar measurements are illustrated in Fig. 2(b). The crystal position was held fixed and the detector separation was held fixed, but both detectors were moved together out of the scattering plane. When both detectors were moved by an aperture radius, no signal was observed, which is expected if the photon pairs were emitted with angles φ and $\varphi + \pi$.

For Fig. 2(c), the crystal position was held fixed; the detectors were kept in the scattering plane, but their separation was changed. Only when $\delta\theta_B$ corresponded to the actual detector separation was a signal observed.

The effects of absorption, finite input beam size, beam collimation, spectral response of the detectors, and electronics were all included in computed theoretical curves. These experimental corrections decreased the signal rate by roughly a factor of 10. Typical signal-loss factors were 3.8 for beam size and collimation, 1.7 for air and other nonsample absorptions, 1.3 for finite energy resolution of the detectors, and 1.12 for dead time of the electronics. To determine the experimental parametric cross section it is necessary to know the flux of input photons. An input flux of 2×10^{7} $\sec^{-1}$ was inferred from the measured flux of Compton-scattered x rays. This calibration technique partially compensates errors in sample and other absorption constants and geometrical effects, because the Compton and parametric scattering efficiencies depend similarly on such effects. The resultant theoretical curves are given as solid lines in Fig. 2. The error bars represent the square root of the total counts. In Fig. 2(a) about 70 counts were accumulated at each of the three peak points, of which about 30 were background. Also in Fig. 2(a) one should note the possible existence of a small signal at $\delta\theta_B = -10'$. Bragg reflection studies indicated a small misoriented crystallite in the Be crystal at the corresponding angle.

The systematic experimental error was anticipated to be about 40%. The quantitative agreement is closer than anticipated. Both the quantitative agreement with calculations and the qualitative agreement with energy-momentum-conservation considerations force identification of the observed process with parametric x-ray conversion. Nonlinear effects involving x-ray and

visible photons have been considered.[7,8] The study of such nonlinearities will provide a valuable probe of material properties.

Our thanks to I. Freund, B. Levine, and P. M. Platzman for helpful discussions, and to W. C. Marra and A. Passner for help on numerous occasions.

[1]S. E. Harris, M. K. Oshman, and R. L. Byer, Phys. Rev. Lett. 18, 732 (1967).

[2]D. A. Kleinman, Phys. Rev. 174, 1027 (1968).

[3]I. Freund and B. F. Levine, Phys. Rev. Lett. 23, 854 (1969), and also Opt. Commun. 1, 419 (1970).

[4]J. A. Armstrong, N. Bloembergen, J. Ducuing, and P. S. Pershan, Phys. Rev. 127, 1918 (1962).

[5]Vachaspati, Phys. Rev. 128, 664 (1962).

[6]N. Bloembergen, Proc. IEEE 51, 124 (1963).

[7]P. M. Eisenberger and S. L. McCall, Phys. Rev. A (to be published).

[8]I. Freund and B. F. Levine, Phys. Rev. Lett. 25, 1241 (1970).

Observation of Direct Nonlinear Coupling of Electromagnetic Waves and Electrostatic Waves in a Plasma*

David Phelps, Nathan Rynn, and Gerard Van Hoven
University of California, Irvine, California 92664
(Received 4 January 1971)

Experiments demonstrating resonant nonlinear electromagnetic wave excitation of electron-plasma and ion-acoustic waves in a plasma column are described. Direct verification of the wave-number selection rule and indirect measurements of the mode power levels are shown.

We report the observation of direct second-order nonlinear coupling among electromagnetic (EM) and electrostatic (ES) waves in a potassium plasma column in a Q machine.[1] By the term "direct" we mean that the exciting waves and the interacting waves are the same. The coupling takes place in the volume of the column and not in the boundaries or in a locally resonant layer. The measurements are made under conditions that enable the unambiguous determination of the wavelength, the frequency, the polarization, the field configuration, and the power levels of the interacting waves. Earlier observations of wave-wave interactions in a plasma have been made in a nonuniform volume and have involved electrostatic waves exclusively. The original work of Stern and Tzoar[2] used the Tonks-Dattner resonances, externally driven by EM waves. Later work on Bernstein modes contains a verification of the wave-number selection rules for waves propagating across a plasma column.[3] Plasma-like interactions between electron-stream and slow waveguide waves have also been observed.[4]

It is well known that the lowest- or second-order nonlinearity in the charged-particle response resonantly couples plasma waves, if their fields and currents are not orthogonal, when the vector selection rules

$$\omega_3 = \omega_1 \pm \omega_2, \quad \vec{k}_3 = \vec{k}_1 \pm \vec{k}_2, \tag{1}$$

are satisfied in the plasma volume.[5,6] The kinematic character of the interaction depends upon the energy densities and group velocities.[7]

As shown schematically in Fig. 1, the Q machine produces a plasma column with a typical density of 10^{10} cm^{-3} in an axial magnetic field of 5 kg. A cylindrical microwave cavity, 35 cm long by 10 cm in diameter, which can be excited in two resonant modes simultaneously, surrounds the 2-cm-diam plasma column. Axially movable coupling probes detect electron and ion waves and make possible the determination of wavelength. The interferometer system used to detect the interactions is similar, with the addition of a nonlinearly generated reference, to that described in greater detail elsewhere.[8] The phase coherence of the detected signal insures the observation of the desired nonlinear output at the difference frequency.

The electromagnetic and electron-plasma body waves which propagate in this configuration are the normal modes[9] of a cylindrical waveguide, partially filled with a plasma, in a strong magnetic field. The axial-field variation of the TM_{lmn} transverse-magnetic mode is given by

$$(E_z)_{lmn} = \hat{E}_0 J_l(T_m r) \exp[i(\omega_n t - k_n z - l\theta)], \tag{2}$$

in the standard waveguide notation.[10] Most of the experiments were performed with a large-amplitude TM-wave "pump," thereby insuring that the